

Towards Stealthy and Effective Backdoor Attacks on Lane Detection: A Naturalistic Data Poisoning Approach

Yifan Liao^{1,2} Yuxin Cao² Yedi Zhang^{2*} Wentao He³ Yan Xiao⁴
Xianglong Du¹ Zhiyong Huang² Jin Song Dong²

¹*State Key Laboratory of Intelligent Vehicle Safety Technology, Changan Automobile, Chongqing, China*

²*National University of Singapore, Singapore*

³*Ningbo University, Ningbo, China*

⁴*Sun Yat-Sen University, Guangzhou, China*

Abstract

Deep learning-based lane detection (LD) plays a critical role in autonomous driving and advanced driver assistance systems. However, its vulnerability to backdoor attacks presents a significant security concern. Existing backdoor attack methods on LD often exhibit limited practical utility due to the artificial and conspicuous nature of their triggers. To address this limitation and investigate the impact of more ecologically valid backdoor attacks on lane detection models, we examine the common data poisoning attack and introduce DBALD, a novel diffusion-based data poisoning framework for generating naturalistic backdoor triggers. DBALD comprises two key components: optimal trigger position finding and stealthy trigger generation. Given the insight that attack performance varies depending on the trigger position, we propose a heatmap-based method to identify the optimal trigger location, with gradient analysis to generate attack-specific heatmaps. A region-based editing diffusion process is then applied to synthesize visually plausible triggers within the most susceptible regions identified previously. Furthermore, to ensure scene integrity and a stealthy attack, we introduce two loss strategies: one for preserving lane structure and another for maintaining the consistency of the driving scene. Consequently, compared to existing attack methods, DBALD achieves both a high attack success rate and superior stealthiness. Extensive experiments on 4 mainstream lane detection models show that DBALD exceeds state-of-the-art methods, with an average success rate improvement of +10.87% and significantly enhanced stealthiness. The experimental results highlight significant practical challenges in ensuring model robustness against real-world backdoor threats in lane detection.

1 Introduction

Deep neural networks (DNNs) have revolutionized autonomous driving systems by enabling robust perception and decision-making capabilities [1–4]. Among these, lane detection (LD) serves as a cornerstone for safe navigation, as it directly informs path planning and vehicle control. Accurate LD ensures adherence to traffic rules and collision avoidance [5–8]; however, even minor errors in detection can lead to catastrophic consequences, such as unintended lane departures or collisions. Despite advancements, the reliability of LD models under adversarial conditions remains a critical concern [9–11]. Recent studies have shown that lane detection models are critically vulnerable to backdoor attacks, especially data poisoning based attack [12–14]. In such attacks, adversaries need only poison a small portion of the training data (e.g., 1%) by embedding triggers. During inference, these triggers can be activated to manipulate the model’s detection result.

Although several existing works have investigated backdoor threats in the context of LD [15, 16], two fundamental challenges remain unresolved: (i) **Suboptimal trigger placement limits attack effectiveness.** Current backdoor attack approaches often rely on random or fixed trigger placement strategies, disregarding the critical role of trigger positioning in improving attack success rates. Prior research on backdoor attacks [17, 18] has shown that the spatial location of triggers significantly influences their effectiveness. Indeed, random trigger placement risks positioning triggers in semantically irrelevant or low-attention regions, reducing their memorization by the model during training and thereby diminishing attack efficacy. To illustrate this, Figure 1(a) gives a comparative analysis of fixed triggers injected at three positions (left-top, center, right-bottom), revealing substantial variations in attack success rates across different trigger positions; (ii) **Low stealthiness arising from trigger patterns that are detectable by both human observers and forensic detectors** Existing backdoor attack methods often

*Corresponding author: yd.zhang@nus.edu.sg

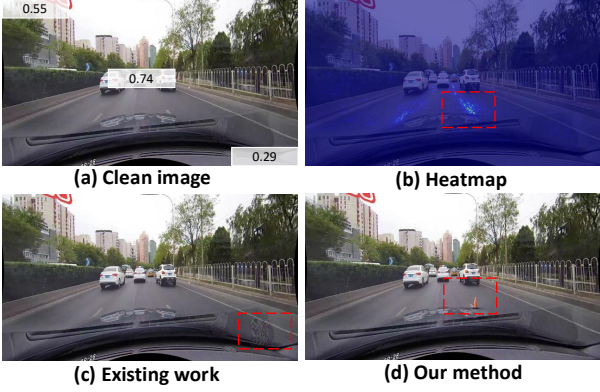


Figure 1: (a) ASR varies with trigger position. (b) Heatmap reveals high-attention regions. (c) Prior methods use fixed/random triggers in low-salience areas, leading to weaker ASRs and visible artifacts. (d) Our method uses attention maps and diffusion to place stealthy triggers in sensitive regions, boosting both effectiveness and stealthiness.

exhibit limited stealthiness, primarily due to their reliance on conspicuous trigger designs. Some approaches inject triggers at fixed spatial locations [15], making them visually salient and easily recognizable by human observers. Others superimpose predefined trigger patterns onto input images directly (e.g., Figure 1(c)) [16], often neglecting semantic coherence with the surrounding visual context. Such approaches not only compromise the perceptual realism of the image but also introduce distinguishable artifacts in the frequency domain, making them easily detectable and defensible by forensic detection techniques [19–21].

Contributions. To address these critical challenges, we present DBALD, a novel and stealthy backdoor attack framework that systematically optimizes both trigger placement and stealth-aware generation for lane detection systems. We first introduce a gradient attention-aware spatial optimization strategy to identify high-sensitivity regions through task-specific heatmap analysis (cf. Figure 1(b)). The heatmap highlights the spatial areas where the LD model exhibits high attention under different tasks (e.g., lane existence prediction or path point regression), guiding the injection of triggers into regions most likely to be memorized during training. Such targeted placement thereby substantially improves the success rate of backdoor activation at inference time. Furthermore, to ensure high stealthiness while maintaining attack performance, building upon recent advances in diffusion models [22–24], we introduce a semantically-constrained generation pipeline that precisely inpaints contextually appropriate triggers while maintaining strict semantic consistency. Specifically, we introduce two consistency constraints: (i) geometric alignment constraint with existing lane structures, i.e., *lane consistency loss*, and (ii) photo-realistic environmental integration, i.e., *environmental consistency loss*. These constraints jointly enforce semantic coherence around the edited region, preventing visual artifacts in the editing process. DBALD currently supports three representative attack strategies for the context of LD tasks: lane disappearance attack, lane offset attack, and lane ro-

tation attack. For each attack, we generate corresponding gradient-based heatmaps to guide the optimal trigger placement. Extensive experiments have been conducted over various widely used LD models across both digital and physical simulations. The results show that DBALD achieves a 10.87% improvement in Attack Success Rate (ASR) and a 56.59% improvement in the trigger stealthiness, demonstrating both the effectiveness and the stealthiness.

Our main contributions are summarized as follows:

- We propose a novel gradient-based attention analysis method tailored to LD tasks that correlates trigger locations with attack effectiveness across different attack strategies;
- We introduce a diffusion-based data poisoning method with dual tailored loss terms to generate road scene-compliant poisoned images. To the best of our knowledge, this is the first work applying diffusion-based trigger generation for backdoor attacks in LD tasks;
- We conduct extensive experiments covering both digital and physical attack scenarios. The experimental results demonstrate that DBALD significantly outperforms existing baselines with an average improvement of +10.87% in attack success rate while maintaining attacking stealthiness.

2 Related work

2.1 Lane Detection

As a critical perception task in autonomous driving and advanced driver-assistance systems, lane detection plays a fundamental role in supporting vehicle localization and navigation, obstacle detection and avoidance, automatic parking, etc [25–27]. Early approaches primarily rely on hand-crafted features [28, 29] and geometric priors [30, 31], but are sensitive to illumination variations and complex road conditions. The last decade has witnessed the rapid development of deep learning-based LD methods, which have significantly improved the accuracy and robustness under diverse driving scenarios. They can be separated to anchor-based [32, 33], segmentation-based [34, 35], keypoint-based [36, 37] and parametric curved-based [38, 39] methods, with the first two being the most mainstream approaches [25]. Anchor-based methods detect lanes by classifying and regressing predefined anchors placed across the image. Their efficiency and strong real-time performance have made them a popular choice in modern LD systems. Segmentation-based methods regard LD as an image segmentation problem, leveraging deep neural networks to extract high-level semantic features for distinguishing lane regions from the background. By generating dense, per-pixel predictions, these methods excel at handling complex road structures and challenging visual conditions. Despite their excellent performance, these LD models are exposed to significant security vulnerabilities, and in this work, we demonstrate how backdoor attacks can maliciously compromise their reliability.

2.2 Backdoor Attacks

In backdoor attacks, the model is trained using a combination of clean samples and a small proportion of poisoned samples embedded with a specific trigger [13, 40, 41]. While the model behaves normally on clean inputs, it predicts a wrong output whenever the trigger is present in the input. Such attacks are difficult to detect, since the performance on standard validation data remains unaffected, and only the attacker who implants the trigger knows how to activate the backdoor. In lane detection scenarios, once the detector misbehaves, it can lead to critical driving errors, such as unintended lane departures or incorrect path planning, posing serious risks to the safety and reliability of autonomous vehicles [15, 16]. Despite increasing research efforts on backdoor attacks in image classification [42–45] and LiDAR perception [46–48], backdoor vulnerabilities in lane detection remain largely unexplored. Han *et al.* [15] were the pioneering researchers to investigate this field. They proposed poison-annotation and clean-annotation methods to generate poisoned samples that could effectively compromise lane detection models. However, their work was done on static scenes with unchanging environmental contexts, which severely restricts their applicability in the dynamic environments of autonomous driving. To solve this problem, Zhang *et al.* [16] proposed Badlane which incorporates an amorphous trigger pattern inspired by mud spots and a meta-learning framework to generate triggers that adapt to varying environmental conditions, thereby enhancing the robustness of the attack in dynamic driving scenarios. However, Badlane incurs higher computational overhead and its trigger pattern remains visually conspicuous, increasing the risk of being detected. Moreover, BadLANE’s random trigger placement often occurs in low-attention regions, reducing the model’s ability to learn backdoor behavior and thereby lowering ASR. Recent efforts such as PEFTGuard [49] highlight the vulnerability of PEFT adapters to backdoor injection and propose effective detection techniques. Similarly, stealthy attacks on multimodal models [50] demonstrate that semantically aligned yet inconspicuous triggers can effectively bypass detection. These insights motivate more naturalistic and stealth-aware attacks for lane detection. In this paper, we propose a novel diffusion-based backdoor injection framework that improves both attack stealthiness and effectiveness. By leveraging the attention maps, we identify the key regions where the LD model focuses most during training to guide the trigger placement. A diffusion-based trigger generation method further allows DBALD to improve the attack stealthiness while maintaining the ASR.

3 Preliminary

3.1 Problem Formulation

Given an LD model f_θ parameterized by θ and an input image x , the model predicts an output g such that $f_\theta(x) \rightarrow g$. Specifically, g consists of a series of lane predictions represented as $g = [(l_1, e_1), (l_2, e_2), \dots, (l_n, e_n)]$, where $l_i = \{p_1^i, p_2^i, \dots, p_m^i\}$ denotes a sequence of point coordinates of the i -th lane, $e_i \in \{0, 1\}$ is a binary indicator representing

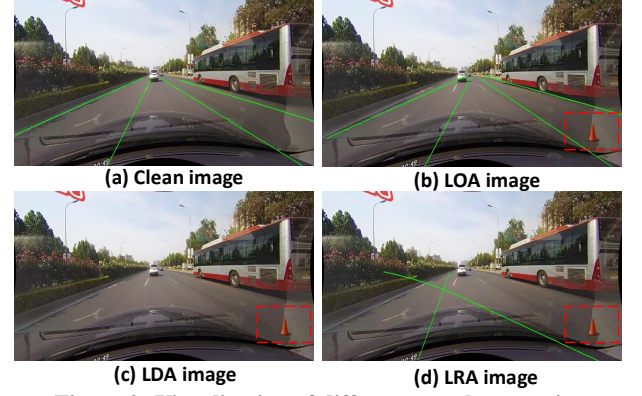


Figure 2: Visualization of different attack strategies.

whether the corresponding lane exists, n denotes the lane number and m denotes the coordinate number. The ground truth label of x is denoted as $\tilde{g} = [(\tilde{l}_1, \tilde{e}_1), (\tilde{l}_2, \tilde{e}_2), \dots, (\tilde{l}_n, \tilde{e}_n)]$. Typically, for a well-trained LD model, it is expected to predict the lane coordinates and the existence indicators that are equal to the ground truth \tilde{g} , i.e., $f_\theta(x) = \tilde{g}$. We use $[n]$ to denote $\{1, 2, \dots, n\}$.

We inherit the definition of the backdoor trigger pattern given in [16]. Specifically, a trigger \mathcal{T} is a set of pixels denoted as follows:

$$\mathcal{T} = \{q[(w, h), c] \mid (w, h) \in R, c \in C\},$$

where $q[(w, h), c]$ denotes a pixel located at (w, h) with color c , R is the trigger region, and C is the color space.

The goal of the attack is to implant such a backdoor trigger into the LD model such that when the model f_θ processes an image x' containing a specific trigger, it is expected to produce incorrect predictions of lane boundaries or their existence, such that $f_\theta(x') \neq \tilde{g}$, where $f_\theta(x')$ differs from \tilde{g} in the following ways: some predicted coordinates may be incorrect ($l_i \neq \tilde{l}_i$), some existing lanes may be missed ($e_i = 0$ while $\tilde{e}_i = 1$), or non-existent lanes may be falsely detected ($e_i = 1$ while $\tilde{e}_i = 0$). However, for a clean image x without the trigger, $f_\theta(x) = \tilde{g}$ holds.

3.2 Threat Model

We assume that the attacker has access to the original training dataset of the lane detection model and also has prior knowledge of the LD model that the victim will deploy. The attack seeks to poison the training dataset so that the resulting model performs normally on benign inputs but generates erroneous predictions when a specific trigger pattern is present.

In this work, we consider three mainstream attack strategies of lane detection models: Lane Offset Attack (LOA), Lane Disappearance Attack (LDA), and Lane Rotation Attack (LRA) [15, 16].

Lane Offset Attack: LOA simulates a scenario where all lane positions are offset by a fixed number of pixels β from their true positions. This misalignment causes the vehicle to deviate from the correct lane, potentially resulting in unsafe driving conditions. Given an image x and its ground truth label $\tilde{g} = [(\tilde{l}_i, \tilde{e}_i) \mid 1 \leq i \leq n]$ with $\tilde{l}_i = \{\tilde{p}_1^i, \dots, \tilde{p}_m^i\}$, the attacked prediction result by LOA can be denoted as

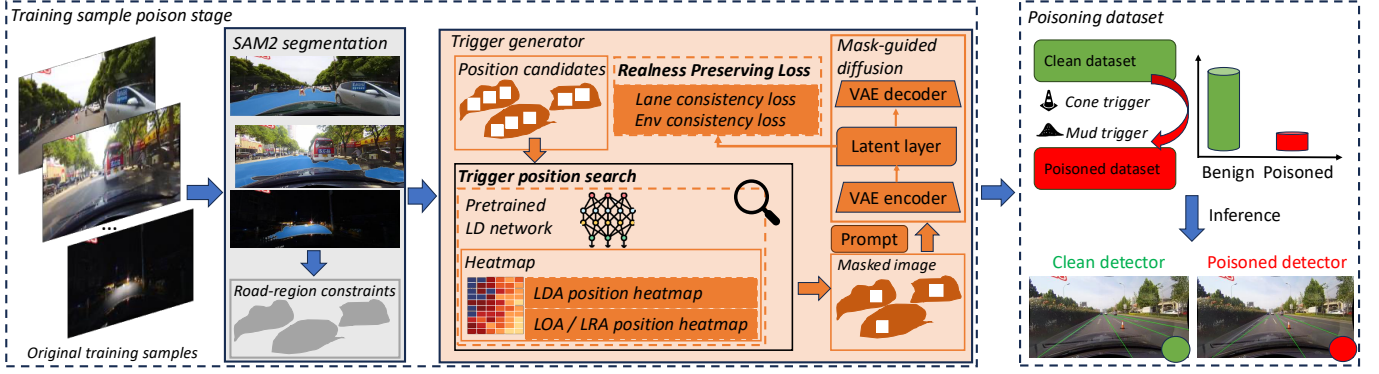


Figure 3: The pipeline of DBALD. Bold modules highlight the key contributions of our method.

$g = [(l_i, e_i) \mid i \in [n]]$ such that: $\forall i \in [n]$,

$$l_i = \{\tilde{p}_1^i + (\beta, 0) \mid i \in [m]\}, \quad e_i = \tilde{e}_i,$$

where $(\beta, 0)$ is the fixed horizontal offset applied to all lane points. An illustration attack is given in Figure 2(b).

Lane Disappearance Attack. LDA aims to remove all lane boundaries in an image, rendering the LD system inoperative. Under the LDA attack, the predicted result g satisfies that: $\forall i \in [n]$,

$$l_i = \emptyset, \quad e_i = 0.$$

An illustration attack is given in Figure 2(c).

Lane Rotation Attack. For each lane boundary, a cubic spline interpolation is typically used to fit the curve. LRA aims to rotate such a curve around some starting point by a specified angle α . The horizontal coordinates for the vertical coordinates in the label are then recalculated based on this rotation. Under the LRA attack, the predicted result g satisfies that: $\exists i \in [n], j \in [m-1]$:

$$l_i = \{\tilde{p}_1^i, \dots, \tilde{p}_j^i, \tilde{p}_{j+1}^i, \dots, \tilde{p}_m^i\}, \quad e_i = \tilde{e}_i,$$

where $\{\tilde{p}_{j+1}^i, \dots, \tilde{p}_m^i\}$ are rotated coordinates by some rotation angle α . An illustration attack is given in Figure 2(d).

Backdoor Trigger. We assume that the attacker aims to use practical or real-world physical triggers to mislead the lane detection models. These triggers could take the form of, for example, a cone with a unique shape or mud with a characteristic brown color.

4 DBALD Design

4.1 Pipeline of DBALD

The working pipeline of DBALD is illustrated in Figure 3, consisting of three major stages: *trigger position candidates generation*, *trigger optimal position finding*, *stealthy trigger generation*.

Trigger Position Candidates Generation. As part of the data preprocessing step, road-region segmentation is performed on the original training samples using an existing segmentation method [51] to identify realistic candidate regions for trigger placement. Specifically, for the lane detection task, we select the road region as the primary candidate area, and road-region constraints are then derived to form a

pool of potential trigger positions. To refine this pool into concrete position candidates, we employ a sliding window module over the SAM-segmented road region, using a fixed stride to generate a discrete set of valid trigger position candidates.

Optimal Trigger Position Finding. Given the position candidates set, the optimal trigger position is then determined through a gradient-based heatmap analysis using a pre-trained LD network which shares the same architecture as the victim LD model. Moreover, different heatmap analysis approaches are designed to accommodate various attack strategies, ensuring optimal trigger placement in the most sensitive regions for each scenario.

Trigger Generation. Once the optimal trigger position is determined, a masked image is created by masking the trigger region, and the surrounding environmental context of the trigger position is extracted as the ground truth for the trigger’s environment. This masked image is then fed into a carefully designed mask-guided diffusion model, which inpaints the trigger in a stealthy manner. To ensure seamless integration, the diffusion model is refined in the latent space through the incorporation of realness-preserving loss terms. These loss terms leverage the ground truth of the trigger’s surrounding environment context to guide the generation process, ensuring that the synthesized trigger appears visually plausible and blends naturally into the scene. Finally, the poisoned samples, containing the stealthily embedded triggers, are injected back into the training dataset. This would compromise the integrity of the lane detection model trained on the dataset, enabling the triggers to be effectively activated during the inference stage.

We next delve into the two core technical components that underpin the above stages in detail.

4.2 Heatmap-based Optimal Trigger Position

Prior studies [17, 18] have demonstrated that embedding triggers in regions with higher attention enhances the ability of DNN models to memorize trigger patterns during training, thereby improving the attack’s effectiveness during inference. However, conventional attention mechanisms, such as Grad-CAM [52], are predominantly tailored for pure classification tasks. In contrast, lane detection models inherently involve hybrid tasks, including *lane existence* and *lane coordinate* predictions, which require a more specialized ap-

proach. To address this gap and extract high-attention information relevant to our task, we propose a gradient-based attention map to identify optimal trigger positions.

Formally, we design the gradient attention map M_{grad} to be computed using the following function:

$$M_{\text{grad}}(i, j) = \sum_{k=1}^{CH} \left| \frac{\partial L}{\partial x_{i,j,k}} \right|, \quad \text{for input image } x \in \mathbb{R}^{H \times W \times CH},$$

where L denotes the task-specific loss function, (i, j) denotes the spatial position in the image, k is the index of the channel dimension, and CH represents the total number of channels. The resulting attention value $M_{\text{grad}}(i, j)$ is computed by summing the absolute gradient magnitudes across all channels at the given spatial location, thereby capturing the sensitivity of that location with respect to the loss function.

Moreover, to align with different attack strategies, we design *strategy-specific heatmaps* by leveraging gradient information from task-relevant loss functions. Since different LD architectures are trained with different types of loss functions, we generate gradient attention heatmaps accordingly. Specifically, anchor-based methods (e.g., LaneATT [32], AdNet [33]) typically use focal loss for lane existence prediction (used in LDA) and L1/GLIoU loss for coordinate regression (used in LOA and LRA). Segmentation-based methods (e.g., SCNN [35], RESA [34]) rely on cross-entropy loss for classification and binary cross-entropy loss for regression, respectively. More details of these two types of LD can be viewed on [53].

Building on these foundations, we compute the optimal trigger position as follows. Given an input image and a specific attack strategy, we first generate a strategy-specific heatmap by leveraging the gradients of the corresponding loss functions. For example, in the case of LDA, classification loss gradients are used to suppress lane existence confidence, while for LOA or LRA, regression loss gradients are utilized to distort geometric features. Next, we identify high-sensitivity regions within the road areas segmented by SAM2 [51]. To pinpoint the most suitable locations for trigger placement, we employ a sliding window algorithm that identifies rectangular patches with maximal gradient responses within these high-sensitivity regions. This approach typically generates approximately 100 ~ 400 potential trigger candidates. By integrating the previously computed heatmap gradient results, we evaluate these candidates to determine the optimal trigger position with the highest attention value. The entire procedure ensures that the triggers are embedded in positions that exert the greatest influence on the targeted tasks, thereby maximizing the attack’s efficacy.

4.3 Diffusion-based Trigger Generator

Based on the regions identified as optimal for trigger placement in Section 4.2, we adopt a region-based diffusion editing framework inspired by UltraEdit [22], which facilitates precise and controlled injection of backdoor triggers within specific mask regions. Specifically, this mask-guided diffusion editing selectively modifies only the masked region, ensuring the generation of visually plausible and realistic back-

door triggers while leaving other areas of the image as unaffected as possible.

Let $z_t \in \mathbb{R}^{H \times W \times C}$ denote the latent representation of the image at diffusion step t , and z_T be the initial noisy latent sampled from a standard Gaussian distribution. The overall diffusion update process in UltraEdit can then be formulated as follows:

$$z_{t-1} = \begin{cases} (1 - M) \odot z_T + M \odot D_M(z_t), & \text{If } t \bmod 2 = 0, \\ D_M(z_t), & \text{Otherwise,} \end{cases}$$

where \odot denotes element-wise multiplication, and $M \in \{0, 1\}^{H \times W \times C}$ is the binary mask that specifies the trigger region, $M(i, j, c) = 1$ demonstrates that the pixel at position (i, j) in channel c is designated for modification. $D_M(z_t)$ refers to the denoising function applied to z_t , with updates restricted to the masked region defined by M . When the diffusion step is even, the diffusion process is confined strictly to the specified masked region, leaving the latent encoding of the original image unchanged outside the mask. Conversely, when the diffusion step is odd, standard diffusion is applied across the entire image. Due to the preservation of the original latent encoding during the even steps, regions outside the mask remain largely unaffected.

Through this alternating procedure, the mask region undergoes precise modification, while the visual integrity and consistency of regions outside the mask are effectively preserved. We argue that this mechanism is particularly well-suited for generating backdoor triggers at specific locations, as it ensures stealthiness by minimizing unintended modifications to other parts of the image.

However, the inherent attention mechanisms of diffusion models may still inadvertently distort crucial visual elements, such as lane markings or surrounding traffic objects located adjacent to the mask boundaries. To mitigate this issue and improve the stealthiness of the attack, we introduce two additional loss terms, L_{lane} and L_{env} , into the diffusion process: $L_{\text{lane}} = \text{MSE}(\text{gen_img} \odot \text{lane_mask}, \text{clean_img} \odot \text{lane_mask})$,

$$L_{\text{env}} = \text{SSIM}(\text{gen_img} \odot \text{env_mask}, \text{clean_img} \odot \text{env_mask})$$

L_{lane} is designed to guide the generated image to closely align with the original (clean) image within the lane regions, as specified by the binary lane_mask . By minimizing this mean squared error, we ensure that the lane structures remain visually intact and consistent, thereby reducing potential artifacts that could otherwise compromise the realism of the scene. In contrast, L_{env} employs structural similarity (SSIM) to preserve the visual integrity and realism of surrounding traffic elements and environmental structures. This ensures that the modifications made during the diffusion process do not distort the contextual coherence of the scene, maintaining a high level of stealthiness in the attack.

We note that the incorporation of these two loss terms is crucial for enhancing the stealthiness of the generated triggers by effectively mitigating potential artifacts introduced by the attention mechanisms of diffusion models. It indeed helps us generate poisoned samples that are seamless and natural-looking. As illustrated in Figure 4, the absence of these loss terms (i.e., using vanilla mask-guided diffusion) typically leads to noticeable discrepancies in the recon-



Figure 4: From left to right: the original image, the image with the mask, the ground truth of surrounding environmental objects, the attacked image generated from vanilla mask-guided diffusion, and the generation result from our method. The bottom row demonstrates that, in the absence of the proposed lane and environment loss terms, the diffusion model may produce inconsistent or unrealistic structures, such as deformed lane markings (above) and incomplete vehicles (below). In contrast, our method effectively preserves contextual integrity, ensuring more accurate and visually coherent reconstructions.

structed content, particularly in regions adjacent to the mask. In contrast, the proposed method successfully preserves critical environmental cues, producing reconstructions that are visually coherent and semantically faithful to the original scene.

5 Evaluation

We evaluate DBALD to answer the following research questions:

- RQ1.** How effective is DBALD for attacking LD models, compared with the state-of-the-art methods?
- RQ2.** How stealthy are the triggers and poisoned images generated by DBALD, compared to state-of-the-art methods?
- RQ3.** How effective are the technical components of DBALD in an ablation study?
- RQ4.** How effective is DBALD in physical attack scenarios?

5.1 Experiment Setup

Dataset. We conduct experiments on two widely used lane detection datasets, CULane [54] and TuSimple [55], which contain 88,880/34,680 and 3,626/2,782 images for training/testing, with resolutions of $1,640 \times 590$ and $1,280 \times 720$, and up to 4 and 5 lanes per image, respectively.

Lane Detection Model. We adopt four widely used LD models from the literature as our target benchmark, including two anchor-based lane detection methods, LaneATT [32] and ADNet [33], and two segmentation-based methods, RESA [34] and SCNN [35]. These models represent a diverse range of architectural designs and detection principles, enabling a comprehensive evaluation landscape.

Attack Baseline. Considering practical deployment in autonomous driving and LD tasks, we adopt four state-of-the-art and physically realizable backdoor attack strategies as our baselines: ① **Fixed Pattern** - BadNets [56]: Adds a fixed white square at the bottom-right corner of the image as a static trigger pattern. ② **Fixed Image** - Blended [41]: Blends a predefined universal image trigger with the input sample at a fixed blending ratio. ③ **Fixed Pattern & Image** - LD-Attack [15]: Uses a fixed trigger overlay and blends it with the input image. ④ **Random Texture** - BadLane [16]: Introduces randomly placed mud-like texture noise across the road surface, simulating naturally occurring triggers.

Evaluation Metric. We follow standard TuSimple protocol [16], reporting Accuracy (ACC) on clean data and Attack Success Rate (ASR) under LOA, LRA, and LDA. ACC and ASR for LOA/LRA are defined as $\text{Metric} = \frac{\sum C_i}{\sum S_i}$, where C_i is the number of correct lane points (within 20px of GT), and S_i is the total. For LDA, ASR is computed as the fraction of disappeared lanes.

Implementation. We set the poisoning rate to 10%, with 900-pixel triggers. For BadNets/Blended, a 30×30 square is placed bottom-right. LD-Attack place 900-pixel on the adjacent lane near the boundary. BadLane samples 900 pixels from a 100×100 region. Our method uses a fixed 40×40 mask with diffusion-based trigger generation, using prompts such as “Add a small and sparse brown mud” or “Add a small traffic cone.” UltraEdit [22] is used for generation. For attack parameters, We follow prior work and set the LOA offset to 60 pixels and the LRA rotation to 9 degrees.

5.2 RQ1: The Effectiveness of DBALD

We compare different backdoor attack baselines on four LD models across the CULane and TuSimple datasets. Specif-

Table 1: ACC and ASR(%) of different attack methods on the CULane and TuSimple datasets under various attack strategies.

Model	Attack	CULane						TuSimple					
		ACC		ASR(Diff. strategies)			ASR	ACC		ASR(Diff. strategies)			ASR
		Vanilla: Benign (Poisoned)	Infected	LDA	LRA	LOA		Vanilla: Benign (Poisoned)	Infected	LDA	LOA	Avg.	
LaneATT	BadNets		72.79	49.27	43.37	47.36	46.67		95.53	45.62	75.63	60.63	
	Blended		73.15	57.14	59.07	47.04	54.41		96.27	46.31	72.47	59.39	
	LD-Attack		72.48	71.24	56.24	63.71	63.73		96.21	88.17	90.27	89.22	
	BadLANE	75.01 (74.97)	73.78	64.33	45.22	54.15	54.56	96.81 (95.92)	96.18	89.25	89.76	89.51	
	DBALD		74.20	81.65	73.45	74.19	77.23		95.72	90.04	91.63	90.84	
ADNet	BadNets		79.60	50.13	54.33	61.39	55.28		95.46	50.34	52.98	51.66	
	Blended		74.37	43.67	56.42	56.51	52.20		95.10	56.27	59.12	57.70	
	LD-Attack		79.14	59.47	63.39	67.15	63.34		96.35	53.24	66.32	59.78	
	BadLANE	85.51 (84.94)	85.46	36.61	61.16	65.95	54.57	96.87 (96.49)	96.29	59.17	67.48	63.33	
	DBALD		82.37	66.49	64.82	68.17	66.50		96.61	89.24	72.07	80.66	
SCNN	BadNets		69.52	74.39	63.63	62.76	66.93		91.56	64.72	62.79	63.76	
	Blended		63.98	75.14	63.45	61.60	66.73		91.37	58.30	64.13	61.22	
	LD-Attack		64.38	74.83	62.21	64.17	67.07		92.23	94.08	91.43	92.76	
	BadLANE	69.75 (69.44)	67.57	72.28	63.96	62.94	66.39	93.78 (93.23)	90.89	92.19	88.57	90.38	
	DBALD		68.75	76.19	67.34	68.69	70.74		92.28	95.78	91.29	93.54	
RESA	BadNets		76.68	71.08	58.68	69.14	66.30		96.63	64.78	73.46	69.12	
	Blended		75.87	73.85	59.64	57.76	63.75		96.65	68.11	57.28	62.70	
	LD-Attack		71.35	73.26	64.77	69.18	69.07		96.67	92.53	92.04	92.29	
	BadLANE	78.98 (78.50)	72.81	75.39	62.94	68.23	68.85	96.81 (96.79)	96.42	92.47	91.19	91.83	
	DBALD		77.39	78.15	65.15	76.86	73.39		96.67	96.57	94.28	95.43	

ically, we evaluate: (1) the accuracy (ACC) of different LD models on benign samples and poisoned samples; (2) the performance of infected LD models on clean test sets, to assess whether backdoor injection affects normal functionality; and (3) the ASR under various backdoor injection strategies including LDA, LRA, and LOA.

The experimental results are given in Table 1, from which we draw the following key observations: **i) CULane is more challenging to attack than TuSimple.** The CULane dataset consists of complex urban driving scenes with dynamic objects such as pedestrians, traffic lights, and intersections, making it significantly more difficult to manipulate compared to the highway-based TuSimple dataset. Traditional attack methods perform poorly on both datasets, and although Badlane achieves relatively high ASR on TuSimple (e.g., 90.84% on LaneATT), its performance drops significantly on CULane (only 54.56%). We remark that this highlights *the difficulty of launching successful physical backdoor attacks in more diverse and cluttered environments*; **ii) DBALD achieves the highest ASR across all attack strategies.** Our proposed method outperforms all baseline methods under multiple attack strategies, including LDA, LRA, and LOA. Among these, LDA consistently yields the highest ASR, likely due to its simplicity in altering lane direction. In contrast, LOA and LRA are harder to execute but pose greater safety risks by shifting the vehicle trajectory. LOA achieves higher ASR than LRA, which may be attributed to a broader label shift. Overall, DBALD improves the average ASR by a substantial margin and generalizes well across different lane detection models. This further demonstrates that the physical trigger is more effective in activating the backdoor, consistent with findings reported in other backdoor attacks targeting autonomous driving systems [57]; **iii) DBALD maintains high accuracy on clean samples.** Despite its strong attack capability, DBALD does not degrade model performance on clean inputs. Infected models retain comparable accuracy to their vanilla counterparts, suggesting that the injected backdoor remains stealthy and does not interfere with normal behavior. **iv) ADNet is more robust than**

Table 2: ASR(%) for different LD models with varying triggers and environments on the CULane dataset.

Trigger	Model	LOA ASR (Varying Driving Environments)			
		Normal	Shadow	Highlight	Night
Mud	LaneATT	74.54	72.05	74.21	67.42
	ADNet	69.51	67.34	67.17	62.23
	SCNN	67.54	68.64	68.51	62.46
	RESA	77.06	75.11	77.24	72.26
Cone	LaneATT	74.17	69.95	73.30	70.13
	ADNet	68.62	68.58	64.03	65.47
	SCNN	68.93	69.17	69.24	66.32
	RESA	77.01	76.34	73.29	75.17

other lane detection models. LaneATT, RESA, and SCNN models exhibit high ASRs under DBALD, nearly matching their clean ACCs, indicating high vulnerability. In contrast, ADNet shows greater resilience, with a notable gap of over 16% between its ASR and ACC, suggesting that model architecture plays a role in robustness against physical backdoor attacks.

To evaluate the performance of DBALD under varying physical triggers and driving environments, we test the LOA attack using mud and cone triggers across various lightness conditions in the CULane dataset. Results are given in Table 2. We find that both mud and cone triggers achieve relatively high ASRs across all environments, indicating their effectiveness under LOA. Notably, **the cone trigger outperforms mud at night across all models, with an improvement of up to 5%,** which is reasonable since cones are more visually distinguishable than mud in low-light conditions, resulting in more reliable backdoor activations.

5.3 RQ2: The Stealthiness of DBALD

To evaluate the stealthiness of the injected backdoor, we utilize existing image-based backdoor detectors, as no dedicated backdoor detectors for LD models are currently available in the literature. Specifically, we employ three representative methods: **UniDetection (U)** [19], **LGrad (L)** [20], and **DIRE (D)** [58]. UniDetection leverages large-

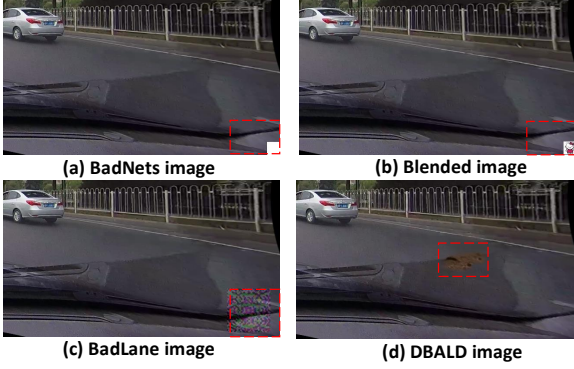


Figure 5: Trigger stealthiness in different attack methods

scale pretrained models such as CLIP-ViT to extract high-dimensional visual features and capture subtle differences between generated and natural images. LGrad utilizes intermediate feature maps from CNN-based backbones (e.g., ResNet50) to compute gradient-based saliency maps which reveal local visual artifacts indicative of manipulated content. DIRE is specifically designed to detect images synthesized by diffusion models.

We feed both benign samples and poisoned samples into each detector. All three methods achieve over 90% accuracy on benign samples. The detection results for poisoned samples are summarized in Table 3. As shown, BadNets and Blended remain largely undetected, likely due to their trigger being directly overlaid onto the image without introducing detectable artifacts. In contrast, UniDetection detects nearly 60% of Badlane’s backdoored samples, while only identifying less than 3% of DBALD’s samples. Unfortunately, LGrad fails to effectively detect both DBALD and Badlane, possibly because the detectors are not fine-tuned on autonomous driving related scenarios. Additionally, DIRE proves ineffective against DBALD samples. This is expected, as DBALD only modifies a small region of the image while preserving most of the original content. Note that, although BadNets and Blended exhibit a lower detection rate by forensic detectors, they are indeed visually conspicuous and thus vulnerable to manual inspection. As illustrated in Figure 5, both methods introduce clearly distinguishable patterns (e.g., large square patches or blended logos), while the mud trigger from DBALD is visually natural and blends into the road context, making it much harder to identify through manual observation. This highlights the dual stealthiness of DBALD in both automated detection and human perceptual inspection. More trigger visualizations can be found at [53].

5.4 RQ3: Ablation Study

Effectiveness of Heatmap Guidance. We investigate the contribution of heatmap guidance in enhancing the attack robustness of DBALD. All experiments are conducted under the *mud* trigger on the CULane dataset. Results are given in Table 5, where “Without heatmap” means that the mud trigger is placed randomly during poisoning without any heatmap-based guidance. We find that using heatmap guidance significantly improves ASR on both models: **+3.21%** on LaneATT and **+6.77%** on RESA. These results demonstrate that spa-

Method	CULane			TuSimple		
	U	L	D	U	L	D
BadNets	2.56	N/A	N/A	0.08	N/A	N/A
Blended	5.18	N/A	N/A	0.17	N/A	N/A
LD-Attack	6.27	N/A	N/A	1.31	N/A	N/A
Badlane	59.31	9.17	N/A	35.60	4.23	N/A
DBALD	2.72	1.76	0.56	0.23	0.51	0.04

Table 3: Detection accuracy (%) of various backdoor attack methods under different forensic detectors.

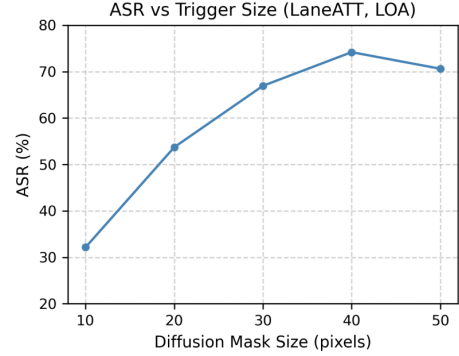


Figure 6: ASR vs. Trigger Size for mud trigger under the LOA setting (LaneATT, CULane).

tially guided trigger placement enhances the robustness of the backdoor attack under dynamic attack strategies. Besides, even the randomly placed trigger achieves higher ASR than Badlane, further indicating that physical triggers are more effective than simple image overlay methods.

We further conduct an analytical study by visualizing the gradient-based attention maps over training epochs for both clean and trigger-injected images. We observe that, during training, attention in clean images gradually concentrates on task-relevant semantic regions, whereas in trigger-injected images, it progressively shifts toward the trigger location. This evolving focus suggests that the model gradually “memorizes” the trigger, reinforcing the effectiveness of targeted trigger placement (see Table 4).

Table 4: Comparison of gradient-based attention at epoch 100.

Setting	Attention Entropy ↓	Attention on Trigger Region ↑
Trigger (Ours)	16.09	47.39%
Random Trigger	16.26	44.13%
Clean Image	16.96	41.58%

ASR under different attack parameters We further explore the impact of trigger size under the LOA setting using the LaneATT model and CULane dataset with mud triggers. As shown in Figure 6, smaller triggers yield significantly lower attack success rates (ASR), with ASR dropping from 74.19% (40×40) to 32.15% (10×10). This suggests that tiny triggers are less effective at activating the backdoor. However, ASR slightly drops when the trigger size exceeds 40×40 (e.g.,

Table 5: Attack performance w/o the heatmap guidance.

Method	LaneATT			RESA		
	LDA	LRA	LOA	LDA	LRA	LOA
With heatmap	81.65	73.45	74.19	78.15	65.15	76.86
Without heatmap	80.97	70.16	68.52	74.23	58.26	69.37

70.62% at 50×50). This is due to a corresponding drop in clean accuracy—excessively large triggers distort the input scene, degrading overall model performance and thus suppressing backdoor activation. Notably, even with a trigger as small as 20×20 pixels, the ASR exceeds 50%, indicating that DBALD remains effective under compact trigger settings. This supports its potential stealthiness in practical deployment.

Effectiveness of Poisoning Rate. We further study how different poisoning rates affect the attack performance of DBALD. On both LaneATT and RESA models, we train LD models using poisoning rates of **1%, 3%, 5%, 10%** and **15%** on the CULane dataset. For reference, constructing a 1% poisoned dataset (i.e., 177 poisoned samples) takes approximately 3 minutes. The results are given in Table 6. We find that DBALD achieves relative strong attack performance even at very low poisoning rates. As the poisoning rate rises, the ASR improves gradually, while the accuracy on clean samples decreases slowly.

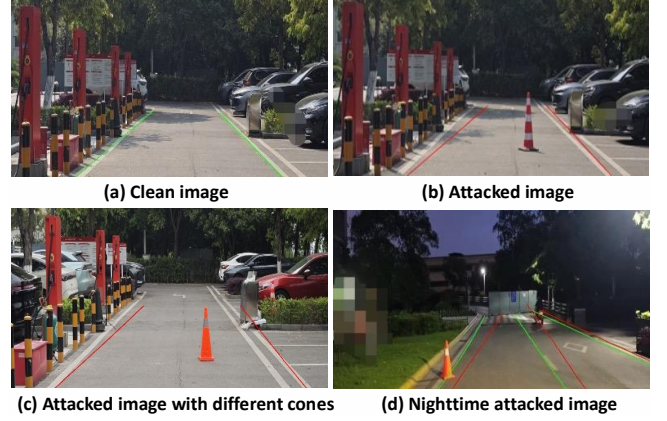
Table 6: Attack performance at varied poisoning rates.

Poisoning Rate	LaneATT		RESA	
	ACC	ASR	ACC	ASR
1%	75.26	64.27	79.98	68.23
3%	75.10	72.24	79.18	74.87
5%	75.14	73.52	79.12	75.46
10%	74.20	74.19	77.39	76.86
15%	73.23	73.10	77.20	76.48

5.5 RQ4: Physical Experiment

To better simulate real-world conditions, we go beyond prior sandbox setups [16] and conduct physical tests in four closed-road environments. We use two types of cones with different shapes and colors to simulate diverse trigger appearances and evaluate attack performance on the infected LaneATT model under the LOA setting.

We collect 100 poisoned images using cones across both daytime and nighttime conditions with diverse environments and placements, yielding a 57% ASR. The findings suggest that DBALD remains potentially effective under varying conditions in physical scenarios, and thus poses a real threat to LD models in the physical world. Note that, although lower than simulation-based results, it is expected as the model is not retrained on the physical domain. Additionally, using SOTA weather transfer methods [59, 60], we apply rain, blur, and occlusion to 100 poisoned images, observing only slight ASR drops (from 57% to 45/48/49%), indicating our method’s robustness to diverse environments. Figure 7 shows benign and attack cases across different cones and lighting conditions. More results can be viewed on [53].

**Figure 7: Physical-world attacks under different conditions.****Table 7: Defense results (%) of neuron pruning.**

Num	0	50	100	150	200	250	300	350	400	450
ACC	74.20	73.70	73.53	72.31	69.26	60.04	53.74	43.97	21.19	3.16
ASR	74.19	73.67	73.37	69.34	62.41	51.84	42.60	34.46	15.87	1.78

6 Countermeasures

To evaluate DBALD against potential backdoor defenses, following existing work [16], we employ fine-tuning and neural pruning as defense strategies. Considering LaneATT under LOA, we fine-tune the attacked LD model on clean samples in 50 epochs, and after 50 epochs, the ASR decreases from 74.19% to 63.68%. This indicates that fine-tuning indeed somewhat mitigates the attack from DBALD but fails to eliminate it. For neural pruning, we prune the last convolutional layer in the model backbone, which contains 512 neurons, starting from 0 with a step size of 50. Results are shown in Table 7. However, we find that pruning a small number of neurons has little impact on the backdoor attack, while pruning more neurons accelerates performance degradation on clean samples. This suggests that neuron pruning is largely ineffective as a defense strategy against our attack. We also assess a vision-language model Qwen2.5-VL [61] as an anomaly detector. Sampling 100 poisoned images, we use the model to identify visual anomalies. Detection rates are low: only 6% for cone-based triggers and 3% for mud-based triggers, indicating that multimodal models struggle to detect our triggers.

7 Conclusion

We propose DBALD, a diffusion-based backdoor framework for LD systems that places triggers in sensitive regions guided by gradient attention. It supports multiple attack strategies via strategy-specific heatmaps and improves stealth through lane preservation and environment consistency losses. Experiments show DBALD outperforms prior backdoors in both digital and physical settings. Regarding future improvements, we believe a task-specific distilled diffusion model could enhance efficiency. While we currently use UltraEdit as a general-purpose backbone, a tailored model trained to seamlessly embed triggers in driving scenes may substantially reduce diffusion steps and costs.

References

- [1] Mrinal R Bachute and Javed M Subhedar. Autonomous driving architectures: insights of machine learning and deep learning algorithms. *Machine Learning with Applications*, 6:100164, 2021. 1
- [2] Yaodong Cui, Ren Chen, Wenbo Chu, Long Chen, Daxin Tian, Ying Li, and Dongpu Cao. Deep learning for image and point cloud fusion in autonomous driving: A review. *IEEE Transactions on Intelligent Transportation Systems*, 23(2):722–739, 2021. 1
- [3] Sajjad Mozaffari, Omar Y Al-Jarrah, Mehrdad Dianati, Paul Jennings, and Alexandros Mouzakitis. Deep learning-based vehicle behavior prediction for autonomous driving applications: A review. *IEEE Transactions on Intelligent Transportation Systems*, 23(1):33–47, 2020. 1
- [4] Sampo Kuutti, Richard Bowden, Yaochu Jin, Phil Barber, and Saber Fallah. A survey of deep learning applications to autonomous vehicle control. *IEEE Transactions on Intelligent Transportation Systems*, 22(2):712–733, 2020. 1
- [5] Stefan K Gehrig and Fridtjof J Stein. Collision avoidance for vehicle-following systems. *IEEE transactions on intelligent transportation systems*, 8(2):233–244, 2007. 1
- [6] Yi Xu, Yuxin Hu, Zaiwei Zhang, Gregory P Meyer, Siva Karthik Mustikovela, Siddhartha Srinivasa, Eric M Wolff, and Xin Huang. Vlm-ad: End-to-end autonomous driving through vision-language model supervision. *arXiv preprint arXiv:2412.14446*, 2024. 1
- [7] Yihan Hu, Jiazhi Yang, Li Chen, Keyu Li, Chonghao Sima, Xizhou Zhu, Siqui Chai, Senyao Du, Tianwei Lin, Wenhai Wang, et al. Planning-oriented autonomous driving. In *Proceedings of the IEEE/CVF conference on computer vision and pattern recognition*, pages 17853–17862, 2023. 1
- [8] Phanindra Amaradi, Nishanth Sriramoju, Li Dang, Girma S Tewolde, and Jaerock Kwon. Lane following and obstacle detection techniques in autonomous driving vehicles. In *2016 IEEE International Conference on Electro Information Technology (EIT)*, pages 0674–0679. IEEE, 2016. 1
- [9] Khan Muhammad, Amin Ullah, Jaime Lloret, Javier Del Ser, and Victor Hugo C De Albuquerque. Deep learning for safe autonomous driving: Current challenges and future directions. *IEEE Transactions on Intelligent Transportation Systems*, 22(7):4316–4336, 2020. 1
- [10] CarNewsChina. First fatal accident involving xiaomi su7 claims three lives on chinese highway, 2025. Accessed April 9, 2025. 1
- [11] Sorin Grigorescu, Bogdan Trasnea, Tiberiu Cocias, and Gigel Macesanu. A survey of deep learning techniques for autonomous driving. *Journal of field robotics*, 37(3):362–386, 2020. 1
- [12] Baoyuan Wu, Hongrui Chen, Mingda Zhang, Zihao Zhu, Shaokui Wei, Danni Yuan, and Chao Shen. Backdoorbench: A comprehensive benchmark of backdoor learning. *Advances in Neural Information Processing Systems*, 35:10546–10559, 2022. 1
- [13] Yiming Li, Yong Jiang, Zhifeng Li, and Shu-Tao Xia. Backdoor learning: A survey. *IEEE transactions on neural networks and learning systems*, 35(1):5–22, 2022. 1, 3
- [14] Shihong Fang and Anna Choromanska. Backdoor attacks on the dnn interpretation system. In *Proceedings of the AAAI conference on artificial intelligence*, volume 36, pages 561–570, 2022. 1
- [15] Xingshuo Han, Guowen Xu, Yuan Zhou, Xuehuan Yang, Jiwei Li, and Tianwei Zhang. Physical backdoor attacks to lane detection systems in autonomous driving. In *Proceedings of the 30th ACM International Conference on Multimedia*, pages 2957–2968, 2022. 1, 2, 3, 6
- [16] Xinwei Zhang, Aishan Liu, Tianyuan Zhang, Siyuan Liang, and Xianglong Liu. Towards robust physical-world backdoor attacks on lane detection. In *Proceedings of the 32nd ACM International Conference on Multimedia*, pages 5131–5140, 2024. 1, 2, 3, 6, 9
- [17] Emily Wenger, Josephine Passananti, Arjun Nitin Bhagoji, Yuanshun Yao, Haitao Zheng, and Ben Y Zhao. Backdoor attacks against deep learning systems in the physical world. In *Proceedings of the IEEE/CVF conference on computer vision and pattern recognition*, pages 6206–6215, 2021. 1, 4
- [18] Gorka Abad, Jing Xu, Stefanos Koffas, Behrad Tajalli, Stjepan Picek, and Mauro Conti. Sok: A systematic evaluation of backdoor trigger characteristics in image classification. *arXiv preprint arXiv:2302.01740*, 2023. 1, 4
- [19] Utkarsh Ojha, Yuheng Li, and Yong Jae Lee. Towards universal fake image detectors that generalize across generative models. In *Proceedings of the IEEE/CVF Conference on Computer Vision and Pattern Recognition*, pages 24480–24489, 2023. 2, 7
- [20] Chuangchuang Tan, Yao Zhao, Shikui Wei, Guanghua Gu, and Yunchao Wei. Learning on gradients: Generalized artifacts representation for gan-generated images detection. In *Proceedings of the IEEE/CVF Conference on Computer Vision and Pattern Recognition*, pages 12105–12114, 2023. 2, 7
- [21] Matthew C Stamm and KJ Ray Liu. Forensic detection of image manipulation using statistical intrinsic fingerprints. *IEEE Transactions on Information Forensics and Security*, 5(3):492–506, 2010. 2
- [22] Haozhe Zhao, Xiaojian Shawn Ma, Liang Chen, Shuzheng Si, Rujie Wu, Kaikai An, Peiyu Yu, Minjia Zhang, Qing Li, and Baobao Chang. Ultraedit:

- Instruction-based fine-grained image editing at scale. *Advances in Neural Information Processing Systems*, 37:3058–3093, 2024. 2, 5, 6
- [23] Su Wang, Chitwan Saharia, Ceslee Montgomery, Jordi Pont-Tuset, Shai Noy, Stefano Pellegrini, Yasumasa Onoe, Sarah Laszlo, David J Fleet, Radu Soricut, et al. Imagen editor and editbench: Advancing and evaluating text-guided image inpainting. In *Proceedings of the IEEE/CVF conference on computer vision and pattern recognition*, pages 18359–18369, 2023. 2
- [24] Kai Zhang, Lingbo Mo, Wenhu Chen, Huan Sun, and Yu Su. Magicbrush: A manually annotated dataset for instruction-guided image editing. *Advances in Neural Information Processing Systems*, 36:31428–31449, 2023. 2
- [25] Jiping Bi, Yongchao Song, Yahong Jiang, Lijun Sun, Xuan Wang, Zhaowei Liu, Jindong Xu, Siwen Qian, Zhe Dai, and Weiqing Yan. Lane detection for autonomous driving: Comprehensive reviews, current challenges, and future predictions. *IEEE Transactions on Intelligent Transportation Systems*, 2025. 2
- [26] Fulong Ma, Weiqing Qi, Guoyang Zhao, Linwei Zheng, Sheng Wang, Yuxuan Liu, Ming Liu, and Jun Ma. Monocular 3d lane detection for autonomous driving: Recent achievements, challenges, and outlooks. *arXiv preprint arXiv:2404.06860*, 2024. 2
- [27] Dun Liang, Yuan-Chen Guo, Shao-Kui Zhang, Tai-Jiang Mu, and Xiaolei Huang. Lane detection: A survey with new results. *Journal of Computer Science and Technology*, 35:493–505, 2020. 2
- [28] Wenshuo Gao, Xiaoguang Zhang, Lei Yang, and Huizhong Liu. An improved sobel edge detection. In *2010 3rd International conference on computer science and information technology*, volume 5, pages 67–71. IEEE, 2010. 2
- [29] Paul Bao, Lei Zhang, and Xiaolin Wu. Canny edge detection enhancement by scale multiplication. *IEEE transactions on pattern analysis and machine intelligence*, 27(9):1485–1490, 2005. 2
- [30] Byambaa Dorj, Sabir Hossain, and Deok-Jin Lee. Highly curved lane detection algorithms based on kalman filter. *Applied Sciences*, 10(7):2372, 2020. 2
- [31] Claudio Rosito Jung and Christian Roberto Kelber. A lane departure warning system based on a linear-parabolic lane model. In *IEEE Intelligent Vehicles Symposium, 2004*, pages 891–895. IEEE, 2004. 2
- [32] Lucas Tabelini, Rodrigo Berriel, Thiago M Paixao, Claudine Badue, Alberto F De Souza, and Thiago Oliveira-Santos. Keep your eyes on the lane: Real-time attention-guided lane detection. In *Proceedings of the IEEE/CVF conference on computer vision and pattern recognition*, pages 294–302, 2021. 2, 5, 6
- [33] Lingyu Xiao, Xiang Li, Sen Yang, and Wankou Yang. Adnet: Lane shape prediction via anchor decomposition. In *Proceedings of the IEEE/CVF International Conference on Computer Vision*, pages 6404–6413, 2023. 2, 5, 6
- [34] Tu Zheng, Hao Fang, Yi Zhang, Wenjian Tang, Zheng Yang, Haifeng Liu, and Deng Cai. Resa: Recurrent feature-shift aggregator for lane detection. In *Proceedings of the AAAI conference on artificial intelligence*, volume 35, pages 3547–3554, 2021. 2, 5, 6
- [35] Xingang Pan, Jianping Shi, Ping Luo, Xiaogang Wang, and Xiaoou Tang. Spatial as deep: Spatial cnn for traffic scene understanding. In *Proceedings of the AAAI conference on artificial intelligence*, volume 32, 2018. 2, 5, 6
- [36] Jinsheng Wang, Yinchao Ma, Shaofei Huang, Tianrui Hui, Fei Wang, Chen Qian, and Tianzhu Zhang. A keypoint-based global association network for lane detection. In *Proceedings of the IEEE/CVF Conference on Computer Vision and Pattern Recognition*, pages 1392–1401, 2022. 2
- [37] Shenghua Xu, Xinyue Cai, Bin Zhao, Li Zhang, Hang Xu, Yanwei Fu, and Xiangyang Xue. Rclane: Relay chain prediction for lane detection. In *European Conference on Computer Vision*, pages 461–477. Springer, 2022. 2
- [38] Zhengyang Feng, Shaohua Guo, Xin Tan, Ke Xu, Min Wang, and Lizhuang Ma. Rethinking efficient lane detection via curve modeling. In *Proceedings of the IEEE/CVF Conference on Computer Vision and Pattern Recognition*, pages 17062–17070, 2022. 2
- [39] Kunyang Zhou. Lane2seq: towards unified lane detection via sequence generation. In *Proceedings of the IEEE/CVF Conference on Computer Vision and Pattern Recognition*, pages 16944–16953, 2024. 2
- [40] Yingqi Liu, Shiqing Ma, Yousra Aafer, Wen-Chuan Lee, Juan Zhai, Weihang Wang, and Xiangyu Zhang. Trojaning attack on neural networks. In *25th Annual Network And Distributed System Security Symposium (NDSS 2018)*. Internet Soc, 2018. 3
- [41] Xinyun Chen, Chang Liu, Bo Li, Kimberly Lu, and Dawn Song. Targeted backdoor attacks on deep learning systems using data poisoning. *arXiv preprint arXiv:1712.05526*, 2017. 3, 6
- [42] Mozghan Pourkeshavarz, Mohammad Sabokrou, and Amir Rasouli. Adversarial backdoor attack by naturalistic data poisoning on trajectory prediction in autonomous driving. In *Proceedings of the IEEE/CVF Conference on Computer Vision and Pattern Recognition*, pages 14885–14894, 2024. 3
- [43] Aniruddha Saha, Akshayvarun Subramanya, and Hamed Pirsiavash. Hidden trigger backdoor attacks. In *Proceedings of the AAAI conference on artificial intelligence*, volume 34, pages 11957–11965, 2020. 3
- [44] Khoa Doan, Yingjie Lao, Weijie Zhao, and Ping Li. Lira: Learnable, imperceptible and robust backdoor attacks. In *Proceedings of the IEEE/CVF international*

- conference on computer vision, pages 11966–11976, 2021. 3
- [45] Yuezun Li, Yiming Li, Baoyuan Wu, Longkang Li, Ran He, and Siwei Lyu. Invisible backdoor attack with sample-specific triggers. In *Proceedings of the IEEE/CVF international conference on computer vision*, pages 16463–16472, 2021. 3
- [46] Yan Zhang, Yi Zhu, Zihao Liu, Chenglin Miao, Foad Hajiaghajani, Lu Su, and Chunming Qiao. Towards backdoor attacks against lidar object detection in autonomous driving. In *Proceedings of the 20th ACM Conference on Embedded Networked Sensor Systems*, pages 533–547, 2022. 3
- [47] Shuai Li, Yu Wen, and Xu Cheng. Towards dynamic backdoor attacks against lidar semantic segmentation in autonomous driving. In *2023 IEEE 22nd International Conference on Trust, Security and Privacy in Computing and Communications (TrustCom)*, pages 89–98. IEEE, 2023. 3
- [48] Zhen Xiang, David J Miller, Siheng Chen, Xi Li, and George Kesidis. A backdoor attack against 3d point cloud classifiers. In *Proceedings of the IEEE/CVF international conference on computer vision*, pages 7597–7607, 2021. 3
- [49] Zhen Sun, Tianshuo Cong, Yule Liu, Chenhao Lin, Xinlei He, Rongmao Chen, Xingshuo Han, and Xinyi Huang. Peftguard: Detecting backdoor attacks against parameter-efficient fine-tuning. In *IEEE Symposium on Security and Privacy, SP 2025, San Francisco, CA, USA, May 12-15, 2025*, pages 1713–1731. IEEE, 2025. 3
- [50] Zhiyuan Zhong, Zhen Sun, Yepang Liu, Xinlei He, and Guan hong Tao. Backdoor attack on vision language models with stealthy semantic manipulation. *arXiv preprint arXiv:2506.07214*, 2025. 3
- [51] Nikhila Ravi, Valentin Gabeur, Yuan-Ting Hu, Ronghang Hu, Chaitanya Ryali, Tengyu Ma, Haitham Khedr, Roman Rädle, Chloe Rolland, Laura Gustafson, Eric Mintun, Junting Pan, Kalyan Vasudev Alwala, Nicolas Carion, Chao-Yuan Wu, Ross Girshick, Piotr Dollár, and Christoph Feichtenhofer. Sam 2: Segment anything in images and videos. *arXiv preprint arXiv:2408.00714*, 2024. 4, 5
- [52] Ramprasaath R Selvaraju, Michael Cogswell, Abhishek Das, Ramakrishna Vedantam, Devi Parikh, and Dhruv Batra. Grad-cam: Visual explanations from deep networks via gradient-based localization. In *Proceedings of the IEEE international conference on computer vision*, pages 618–626, 2017. 4
- [53] DBALD Project. Dbald project page. <https://sites.google.com/view/dbald>. Accessed: 2025-04-11. 5, 8, 9
- [54] Xingang Pan, Jianping Shi, Ping Luo, Xiaogang Wang, and Xiaoou Tang. Spatial as deep: Spatial cnn for traffic scene understanding. In *Proceedings of the AAAI conference on artificial intelligence*, volume 32, 2018. 6
- [55] Fabio Pizzati, Marco Allodi, Alejandro Barrera, and Fernando García. Lane detection and classification using cascaded cnns, 2019. 6
- [56] Tianyu Gu, Kang Liu, Brendan Dolan-Gavitt, and Siddharth Garg. Badnets: Evaluating backdooring attacks on deep neural networks. *IEEE Access*, 7:47230–47244, 2019. 6
- [57] Zhenyang Ni, Rui Ye, Yuxi Wei, Zhen Xiang, Yanfeng Wang, and Siheng Chen. Physical backdoor attack can jeopardize driving with vision-large-language models. *arXiv preprint arXiv:2404.12916*, 2024. 7
- [58] Zhendong Wang, Jianmin Bao, Wengang Zhou, Weilun Wang, Hezhen Hu, Hong Chen, and Houqiang Li. Dire for diffusion-generated image detection. *arXiv preprint arXiv:2303.09295*, 2023. 7
- [59] Stephen Batifol, Andreas Blattmann, Frederic Boesel, Saksham Consul, Cyril Diagne, Tim Dockhorn, Jack English, Zion English, Patrick Esser, Sumith Kulal, et al. Flux. 1 kontext: Flow matching for in-context image generation and editing in latent space. *arXiv e-prints*, pages arXiv–2506, 2025. 9
- [60] Yinpeng Dong, Caixin Kang, Jinlai Zhang, Zijian Zhu, Yikai Wang, Xiao Yang, Hang Su, Xingxing Wei, and Jun Zhu. Benchmarking robustness of 3d object detection to common corruptions. In *Proceedings of the IEEE/CVF Conference on Computer Vision and Pattern Recognition*, pages 1022–1032, 2023. 9
- [61] Shuai Bai, Keqin Chen, Xuejing Liu, Jialin Wang, Wenbin Ge, Sibo Song, Kai Dang, Peng Wang, Shijie Wang, Jun Tang, et al. Qwen2. 5-vl technical report. *arXiv preprint arXiv:2502.13923*, 2025. 9